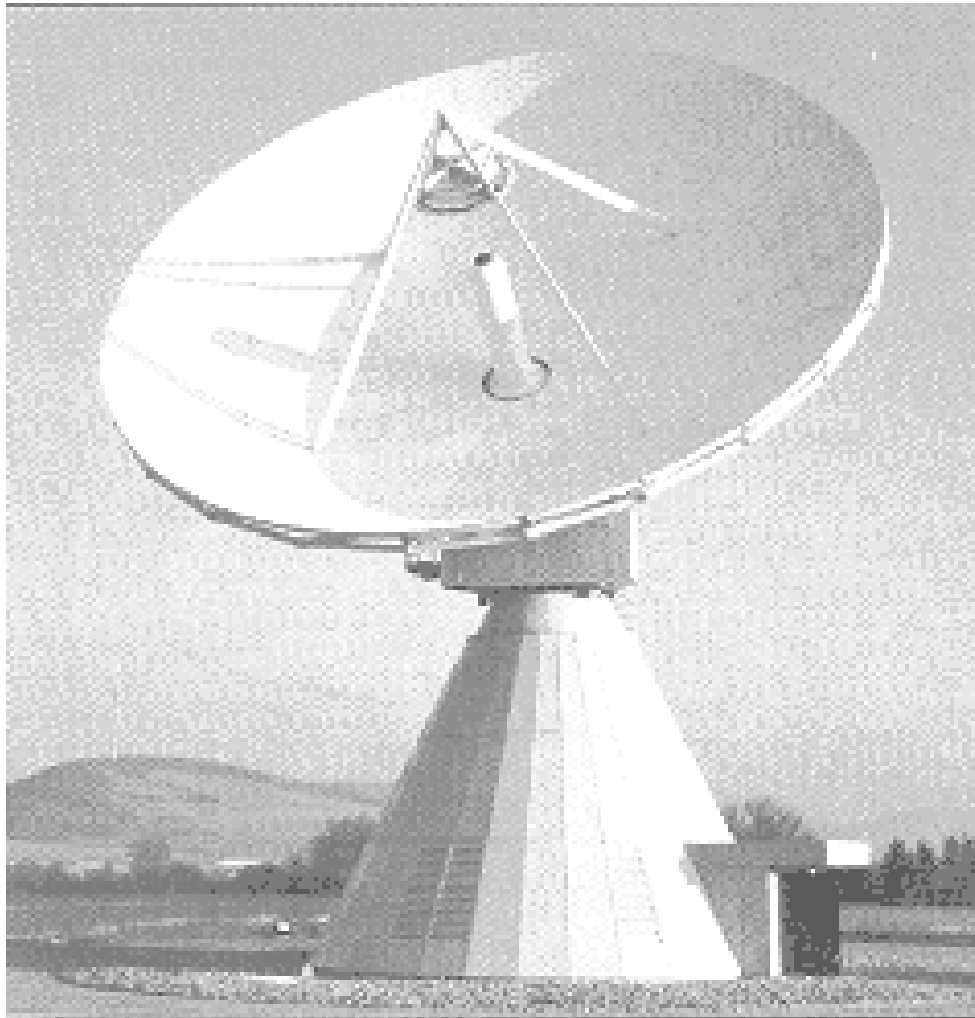


LECTURE 19: Reflector Antennas

1. Introduction

High-gain antennas are required for long-distance radio communications (radio-relay links and satellite links), high-resolution radars, radio-astronomy, etc. Reflector systems are probably the most widely used high-gain antennas. They can easily achieve gains of above 30 dB for microwave and higher frequencies. Reflector antennas operate on principles known long ago from geometrical optics (GO). The first RF reflector system was made by Hertz back in 1888 (a cylindrical reflector fed by a dipole). However, the art of accurately designing such antenna systems was developed mainly during the days of WW2 when numerous radar applications evolved.

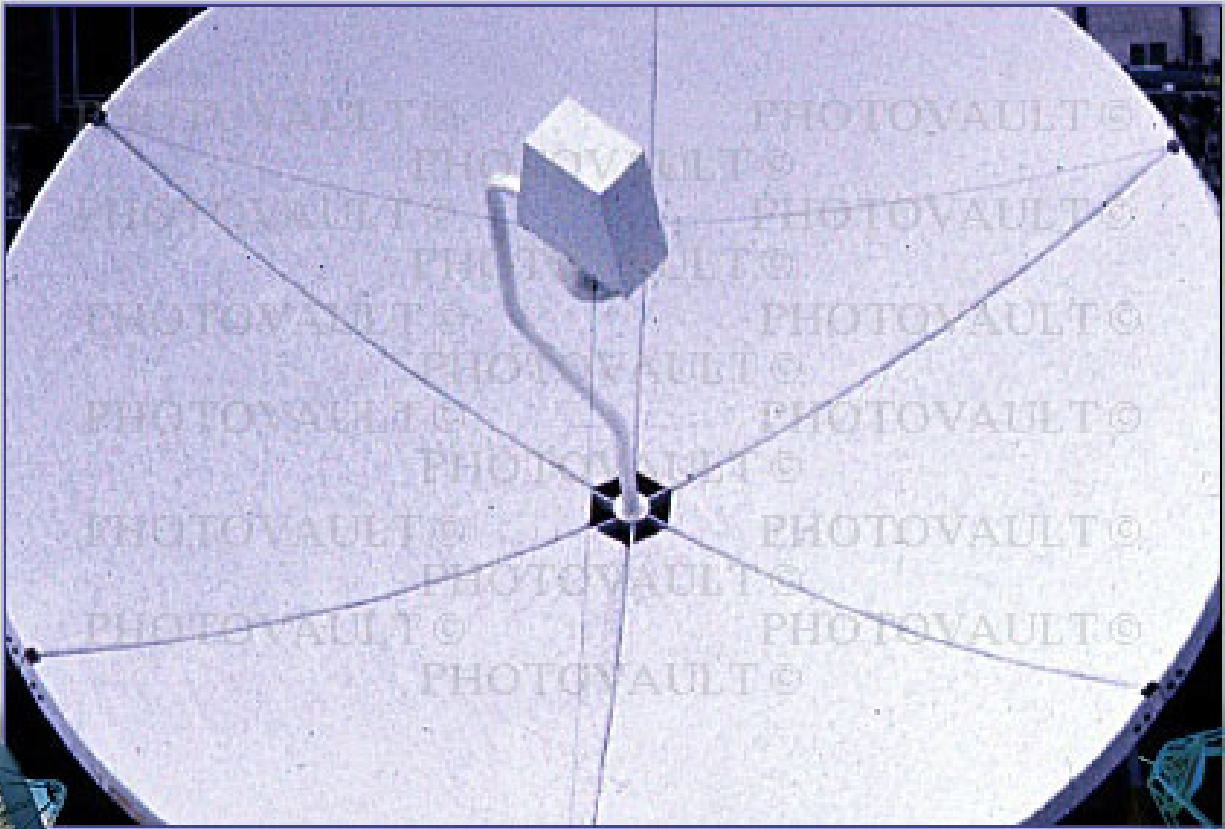
18.3 M INTELSAT EARTH STATION (ANT BOSCH TELECOM), DUAL REFLECTOR



FEED-HORN IS IN FOCAL POINT

San Francisco California

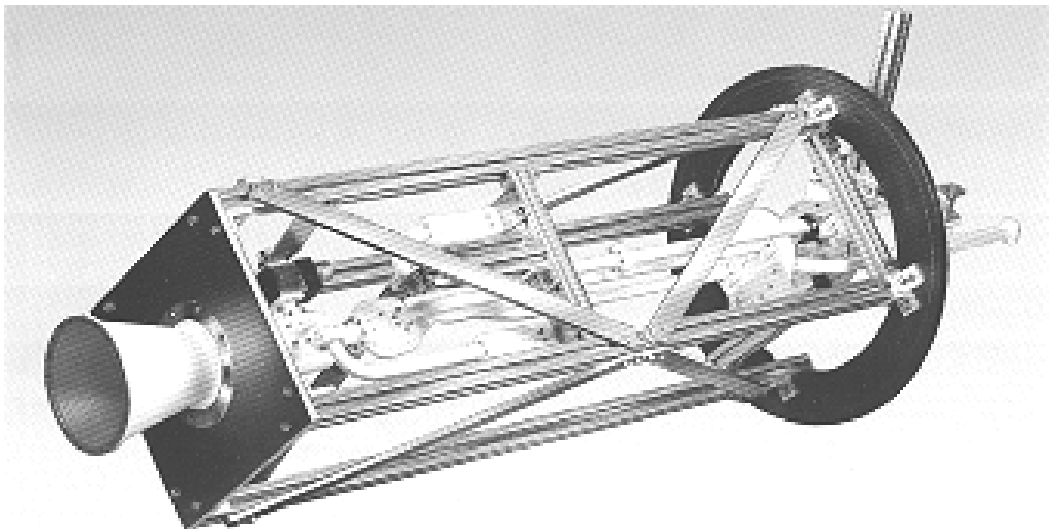
R
a
d
a
r
a
n
d
A
n
t
e
n
n
a
s



I
m
a
g
e
b
y
W
e
r
n
h
e
r
K
r
u
e
i
n

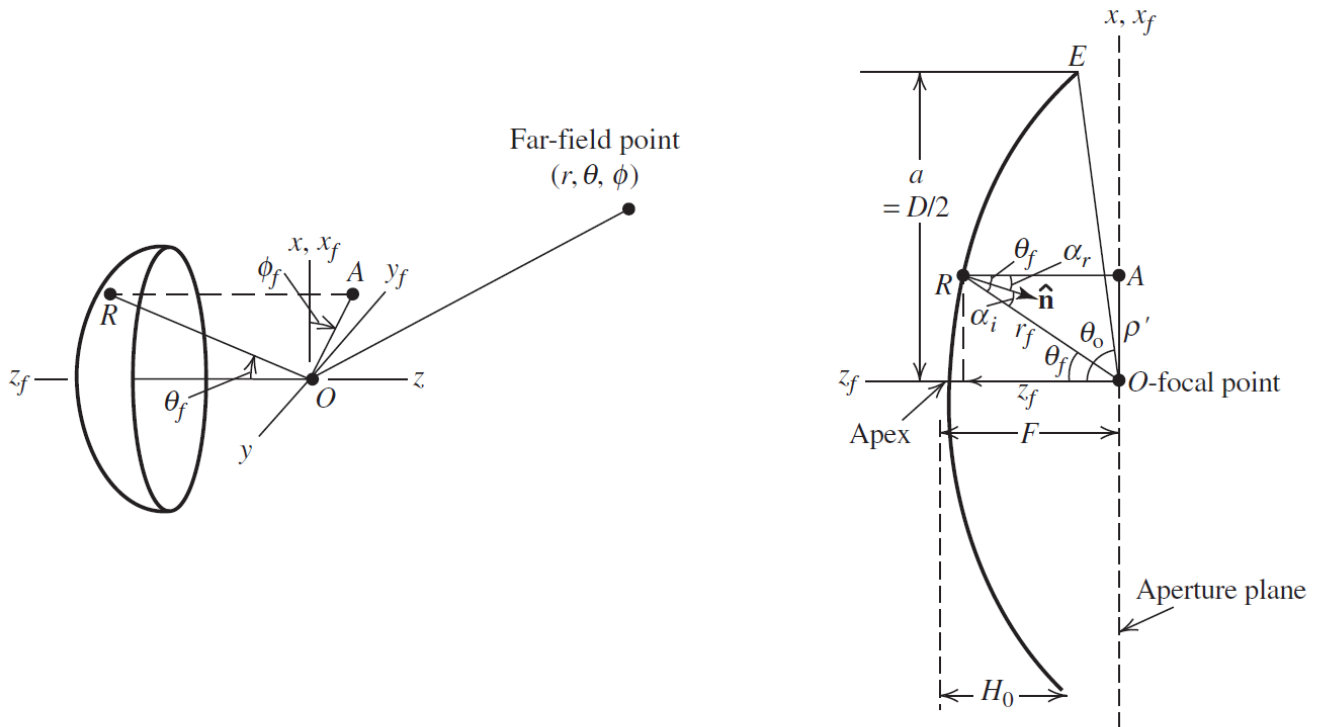
• PHOTOVAULT © •

CONICAL HORN PRIMARY FEED



The simplest reflector antenna consists of two components: a reflecting surface and a much smaller feed antenna at the reflector's focal point. Constructions that are more complex involve a secondary reflector (a subreflector) at the focal point, which is illuminated by a primary feed. These are called dual-reflector antennas. The most common main reflector is the parabolic one. Other common reflectors are: cylindrical, corner, and spherical.

2. Principles of parabolic reflectors



(a) Parabolic reflector and coordinate system.

(b) Cross section of the reflector in the xz -plane.

[Stutzman&Thiele]

A paraboloidal surface is described by the equation (see plot *b*)

$$\rho'^2 = 4F(F - z_f), \quad \rho' \leq a. \quad (19.1)$$

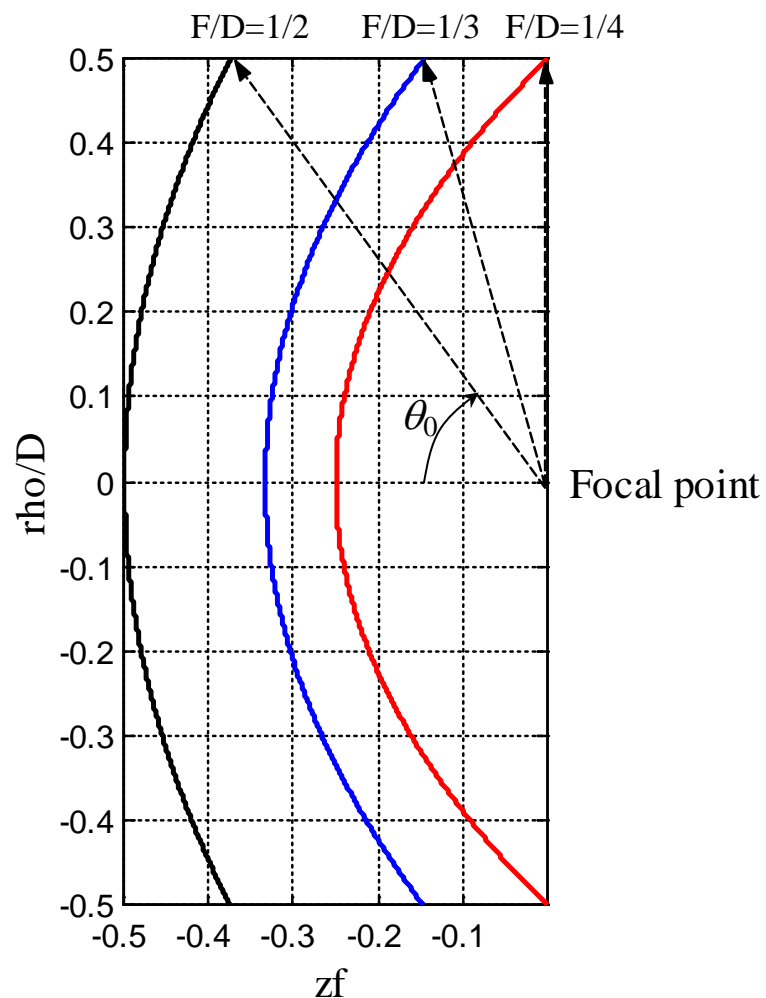
Here, ρ' is the distance from a point A to the focal point O , where A is the projection of the point R on the reflector surface onto the axis-orthogonal plane (the aperture plane) at the focal point. For a given displacement ρ' from the axis of the reflector, the point R on the reflector surface is a distance r_f away from the focal point O . The position of R can be defined either by (ρ', z_f) , which is a rectangular pair of coordinates, or by (r_f, θ_f) , which is a polar pair of coordinates. A relation between (r_f, θ_f) and F is readily found from (19.1):

$$r_f = \frac{2F}{1 + \cos \theta_f} = \frac{F}{\cos^2(\theta_f / 2)}. \quad (19.2)$$

This is the equation of the paraboloidal surface in polar coordinates. Other relations to be used later are:

$$\rho' = r_f \sin \theta_f = \frac{2F \sin \theta_f}{1 + \cos \theta_f} = 2F \tan \left(\frac{\theta_f}{2} \right). \quad (19.3)$$

The axisymmetric (rotationally symmetric) paraboloidal reflector is entirely defined by the respective parabolic line, i.e., by two basic parameters: the diameter D and the focal length F (see plot *b*). Often, the parabola is specified in terms of D and the ratio F/D . When F/D approaches infinity, the reflector becomes flat. Some parabolic curves are shown below. When $F/D = 0.25$, the focal point lies in the plane passing through the reflector's rim.



The angle from the feed (focal) point to the reflector's rim is related to F/D as

$$\theta_0 = 2 \arctan \left[\frac{1}{4(F/D)} \right]. \quad (19.4)$$

The focal distance F of a given reflector can be calculated after measuring its diameter D and its height H_0 (see plot *b*):

$$F = \frac{D^2}{16H_0}. \quad (19.5)$$

Eq. (19.5) is found by solving (19.1) with $\rho' = D/2$ and $z_f = F - H_0$. For example, if $F/D = 1/4$, then $H_0 = D/4 \Rightarrow H_0 = F$, i.e., the focal point is on the reflector's rim plane.

The reflector design problem aims at matching the feed antenna pattern to the reflector. Usually, the feed pattern must be at about a -10 dB level in the direction of the rim, i.e. $\bar{F}_f(\theta = \theta_0) = -10$ dB (0.316 of the normalized amplitude pattern).

The geometry of the paraboloidal reflector has two valuable features:

- All rays leaving the focal point O are collimated along the reflector's axis after reflection.
- All overall ray path lengths (from the focal point to the reflector and on to the aperture plane) are the same and equal to $2F$.

The above properties are proven by the GO methods, therefore, they are true only if the following conditions hold:

- The radius of the curvature of the reflector is large compared to the wavelength and the local region around each reflection point can be treated as planar.
- The radius of the curvature of the incoming wave from the feed is large and can be treated locally at the reflection point as a plane wave.
- The reflector is a perfect conductor, i.e., $\Gamma = -1$.

The collimating property of the parabolic reflector is easily established after finding the unit normal of the parabola,

$$\hat{\mathbf{n}} = \frac{\nabla C_p}{|\nabla C_p|}. \quad (19.6)$$

Here,

$$C_p = F - r_f \cos^2(\theta_f / 2) = 0 \quad (19.7)$$

is the parabolic curve equation [see (19.2)]. After applying the ∇ operator in spherical coordinates, ∇C_p is obtained as

$$\nabla C_p = -\hat{\mathbf{r}}_f \cos^2\left(\frac{\theta_f}{2}\right) + \hat{\boldsymbol{\theta}}_f \cos\left(\frac{\theta_f}{2}\right) \cdot \sin\left(\frac{\theta_f}{2}\right), \quad (19.8)$$

and, therefore,

$$\hat{\mathbf{n}} = -\hat{\mathbf{r}}_f \cos\frac{\theta_f}{2} + \hat{\boldsymbol{\theta}}_f \sin\frac{\theta_f}{2}. \quad (19.9)$$

The angle between $\hat{\mathbf{n}}$ and the incident ray is

$$\cos \alpha_i = -\hat{\mathbf{r}}_f \cdot \hat{\mathbf{n}} = \cos\left(\frac{\theta_f}{2}\right). \quad (19.10)$$

According to Snell's law, $\alpha_i = \alpha_r$. It is easy to show that this is fulfilled only if the ray is reflected in the z -direction:

$$\begin{aligned} \cos \alpha_r = \hat{\mathbf{z}} \cdot \hat{\mathbf{n}} &= \underbrace{(-\hat{\mathbf{r}}_f \cos \theta_f + \hat{\boldsymbol{\theta}}_f \sin \theta_f)}_{\hat{\mathbf{z}}} \cdot \underbrace{\left[-\hat{\mathbf{r}}_f \cos\left(\frac{\theta_f}{2}\right) + \hat{\boldsymbol{\theta}}_f \sin\left(\frac{\theta_f}{2}\right)\right]}_{\hat{\mathbf{n}}} = \\ &= \cos \theta_f \cdot \cos\left(\frac{\theta_f}{2}\right) + \sin \theta_f \cdot \sin\left(\frac{\theta_f}{2}\right) = \cos\left(\frac{\theta_f}{2}\right). \end{aligned} \quad (19.11)$$

Thus, we proved that for any angle of incidence θ_f the reflected wave is z -directed.

The equal-path-length property follows from (19.2). The total path-length L for a ray reflected at the point R is

$$L = \overline{OR} + \overline{RA} = r_f + r_f \cos \theta_f = r_f (1 + \cos \theta_f) = 2F. \quad (19.12)$$

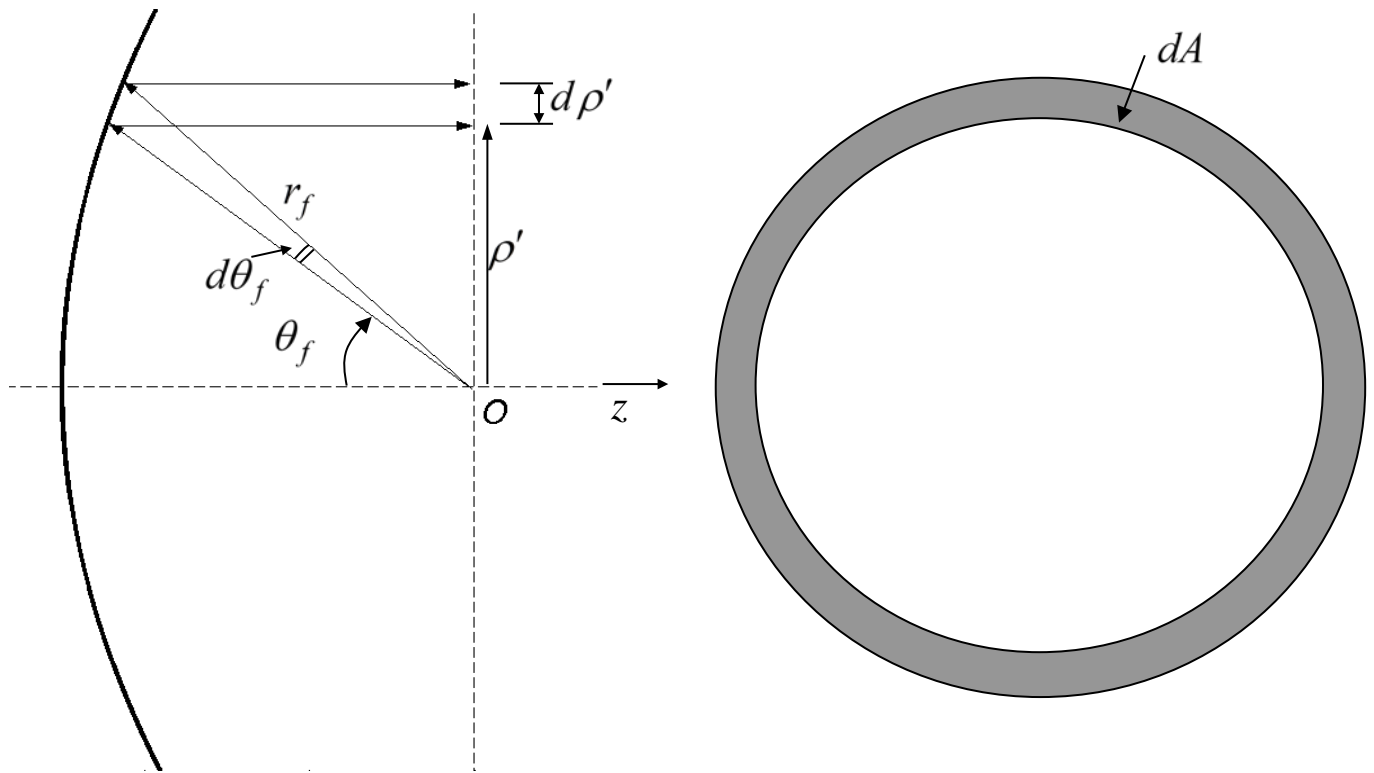
Notice that L is a constant equal to $2F$ regardless of the angle of incidence.

3. Aperture distribution analysis via GO (aperture integration)

There are two basic techniques for the analysis of the radiation characteristics of reflectors. One is called the *current distribution method*, which is a physical optics (PO) approximation. It assumes that the incident field from the feed is known, and that it excites surface currents on the reflector's surface as $\mathbf{J}_s = 2\hat{\mathbf{n}} \times \mathbf{H}^i$. This current density is then integrated to yield the far-zone field. It is obvious that the PO method assumes that the reflector has a perfectly conducting surface and makes use of image theory. Besides, it assumes that the incident wave coming from the primary feed is a locally plane far-zone field.

With the *aperture distribution method*, the field is first found over a plane, which is normal to the reflector's axis, and lies at its focal point (the *antenna aperture*). GO (ray tracing) is used to do that. Equivalent sources are formed over the aperture plane. It is assumed that the equivalent sources are zero outside the reflector's aperture. We first consider this method.

The field distribution at the aperture of the reflector antenna is necessary in order to calculate the far-field pattern, directivity, etc. Since all rays from the feed travel the same physical distance to the aperture, the aperture distribution is of uniform phase. However, there is a non-uniform amplitude distribution. This is because the power density of the rays leaving the feed falls off as $1/r_f^2$. After the reflection, there is practically no spreading loss since the rays are collimated (parallel). The aperture field-amplitude distribution varies as $1/r_f$. This is explained in detail below.



GO assumes that the power density in free space follows straight paths. Applied to the power transmitted by the feed, the power in a conical wedge stays confined within as it progresses along the cone's axis. Consider a conical wedge of solid angle $d\Omega$ whose cross-section angle is $d\theta_f$. It confines power, which after being reflected from the paraboloid, arrives at the aperture plane confined within a cylindrical ring of thickness $d\rho'$ and area $dA = 2\pi\rho'd\rho'$.

Let us assume that the feed is isotropic and it has radiation intensity $U = \Pi_t / 4\pi$, where Π_t is the transmitted power. The power confined in the conical wedge is $d\Pi = Ud\Omega = (\Pi_t / 4\pi)d\Omega$. This power reaches the aperture with a density of

$$P_a(\rho') = \frac{d\Pi}{dA} = \frac{\Pi_t}{4\pi} \frac{d\Omega}{dA}. \quad (19.13)$$

The generic relation between the solid angle increment and the directional-angle increments is

$$d\Omega = \sin\theta d\theta d\varphi, \quad (19.14)$$

(see Lecture 4). In this case, the structure is rotationally symmetric, so we define the solid angle of the conical wedge as

$$d\Omega = \int_0^{2\pi} (\sin \theta_f d\theta_f) d\varphi_f = 2\pi \sin \theta_f d\theta_f. \quad (19.15)$$

The substitution of (19.15) and $dA = 2\pi\rho'd\rho'$ in (19.13) produces

$$P_a(\rho') = \frac{\Pi_t}{4\pi} \frac{2\pi \sin \theta_f d\theta_f}{2\pi\rho'd\rho'} = \frac{\Pi_t}{4\pi} \frac{\sin \theta_f}{\rho'} \frac{d\theta_f}{d\rho'}. \quad (19.16)$$

From (19.3), it is seen that

$$\frac{d\rho'}{d\theta_f} = \frac{F}{\cos^2(\theta_f/2)} = r_f, \quad (19.17)$$

$$\Rightarrow \frac{d\theta_f}{d\rho'} = \frac{1}{r_f}, \quad (19.18)$$

$$\Rightarrow P_a(\rho') = \frac{\Pi_t}{4\pi} \frac{\sin \theta_f}{\underbrace{r_f \sin \theta_f}_{\rho'}} \frac{1}{r_f} = \frac{\Pi_t}{4\pi} \frac{1}{r_f^2}. \quad (19.19)$$

Equation (19.19) shows the spherical nature of the feed radiation, and it is referred to as *spherical spreading loss*. Since $E_a \propto \sqrt{P_a}$,

$$E_a \propto \frac{1}{r_f}. \quad (19.20)$$

If the primary feed is not isotropic, the effect of its normalized field pattern $F_f(\theta_f, \varphi_f)$ is easily incorporated in (19.20) as

$$E_a \propto \frac{F_f(\theta_f, \varphi_f)}{r_f}. \quad (19.21)$$

Thus, we can conclude that the field at the aperture is described as

$$E_a(\theta_f, \varphi_f) = E_m e^{-j\beta 2F} \cdot \frac{F_f(\theta_f, \varphi_f)}{r_f}. \quad (19.22)$$

The coordinates (ρ', φ') are more suitable for the description of the aperture field. Obviously, $\varphi' \equiv \varphi_f$. As for r_f and θ_f , they are transformed as

$$r_f = \frac{4F^2 + \rho'^2}{4F}, \quad (19.23)$$

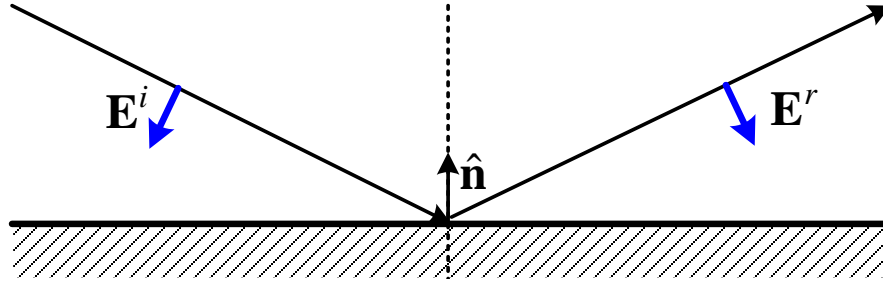
$$\theta_f = 2 \arctan \frac{\rho'}{2F}. \quad (19.24)$$

The last thing to be determined is the polarization of the aperture field provided the polarization of the primary-feed field is known. The law of reflection at a perfectly conducting wall states that $\hat{\mathbf{n}}$ bisects the incident and the reflected rays, and that the total electric field has zero tangential component at the surface, i.e.,

$$\mathbf{E}_\tau^i + \mathbf{E}_\tau^r = 0, \quad (19.25)$$

and

$$\mathbf{E}^r + \mathbf{E}^i = 2(\hat{\mathbf{n}} \cdot \mathbf{E}^i)\hat{\mathbf{n}} \Rightarrow \mathbf{E}^r = 2(\hat{\mathbf{n}} \cdot \mathbf{E}^i)\hat{\mathbf{n}} - \mathbf{E}^i. \quad (19.26)$$



Since $|\mathbf{E}^i| = |\mathbf{E}^r|$, from (19.26), it follows that

$$\hat{\mathbf{e}}_r = 2(\hat{\mathbf{n}} \cdot \hat{\mathbf{e}}_i)\hat{\mathbf{n}} - \hat{\mathbf{e}}_i. \quad (19.27)$$

Here, $\hat{\mathbf{e}}_i$ is the polarization vector of the incident field, and $\hat{\mathbf{e}}_r$ is the polarization vector of the reflected field.

The aperture field distribution is fully defined by (19.22) and (19.27). The radiation integral over the electric field can now be found. For example, a circular paraboloid would have a circular aperture (see Lecture 18), and the radiation integral becomes

$$\mathbf{I}^E = [(\hat{\mathbf{e}}_r \cdot \hat{\mathbf{x}})\hat{\mathbf{x}} + (\hat{\mathbf{e}}_r \cdot \hat{\mathbf{y}})\hat{\mathbf{y}}] E_m \int_0^{2\pi} \int_0^{D/2} \frac{F_f(\rho', \varphi')}{r_f} e^{j\beta\rho' \sin\theta \cos(\varphi - \varphi')} \rho' d\rho' d\varphi'. \quad (19.28)$$

In the above considerations, it was assumed that the aperture field has uniform phase distribution. This is true if the feed is located at the focal point. However, more sophisticated designs often use an offset feed. In such cases, the PO method (i.e., the current distribution method) is preferred.

4. The current distribution (PO) method (surface integration)

The basic description of this approach and its assumptions were already given in the previous section. Once the induced surface currents \mathbf{J}_s are found on the reflector's surface, the magnetic vector potential \mathbf{A} and the far-zone field can be calculated. In practice, the electric far field is calculated directly from \mathbf{J}_s by

$$\mathbf{E}^{far} = -j\omega\mu \frac{e^{-j\beta r}}{4\pi r} \iint_{S_r} \underbrace{[\mathbf{J}_s - (\mathbf{J}_s \cdot \hat{\mathbf{r}})\hat{\mathbf{r}}]}_{\mathbf{J}_{s,\perp\hat{\mathbf{r}}}} e^{j\beta\hat{\mathbf{r}}\cdot\mathbf{r}'} ds'. \quad (19.29)$$

Equation (19.29) follows directly from the relation between the far-zone electric field and the magnetic vector potential \mathbf{A} ,

$$\mathbf{E}^{far} = -j\omega\mathbf{A}_\perp, \quad (19.30)$$

which can be written formally as

$$\mathbf{E}^{far} = -j\omega\mathbf{A} - (-j\omega\mathbf{A} \cdot \hat{\mathbf{r}})\hat{\mathbf{r}} = -j\omega(A_\theta\hat{\boldsymbol{\theta}} + A_\varphi\hat{\boldsymbol{\phi}}). \quad (19.31)$$

This approach is also known as Rusch's method. The integral in (19.29) is usually evaluated numerically by computer codes in order to render the approach versatile with respect to any aperture shape and any aperture current distribution.

In conclusion, we note that both the GO and the PO methods produce very accurate results for the main beam and first side lobe. The pattern far out the main beam can be accurately predicted by including diffraction effects (scattering) from the reflector's rim. This is done by augmenting GO with the use of *geometrical theory of diffraction* (GTD) (J.B. Keller, 1962), or by augmenting the PO method with the *physical theory of diffraction* (PTD) (P.I. Ufimtsev, 1957).

5. The focus-fed axisymmetric parabolic reflector antenna

This is a popular reflector antenna, whose analysis is used here to illustrate the general approach to the analysis of any reflector antenna. Consider a linearly polarized feed, with the \mathbf{E} field along the x -axis. As before, the reflector's axis is along z . Let us also assume that the field of the feed is represented by

$$\mathbf{E}_f(\theta_f, \varphi_f) \approx E_m \frac{e^{-j\beta r_f}}{r_f} \left[\hat{\boldsymbol{\theta}}_f C_E(\theta_f) \cos \varphi_f - \hat{\boldsymbol{\phi}}_f C_H(\theta_f) \sin \varphi_f \right]. \quad (19.32)$$

Here, $C_E(\theta_f)$ and $C_H(\theta_f)$ denote the principal-plane patterns. The expression in (19.32) is a common approximation of a 3-D pattern of an x -polarized antenna by knowing only the two principal-plane 2-D patterns. This approximation is actually very accurate for aperture-type antennas because it directly follows from the expression of the far-zone fields in terms of the radiation integrals (see Lecture 17, Section 4):

$$E_\theta = j\beta \frac{e^{-j\beta r}}{4\pi r} [I_x^E \cos \varphi + I_y^E \sin \varphi + \eta \cos \theta (I_y^H \cos \varphi - I_x^H \sin \varphi)], \quad (19.33)$$

$$E_\varphi = j\beta \frac{e^{-j\beta r}}{4\pi r} [-\eta (I_x^H \cos \varphi + I_y^H \sin \varphi) + \cos \theta (I_y^E \cos \varphi - I_x^E \sin \varphi)]. \quad (19.34)$$

The aperture field is now derived in terms of x - and y -components. To do this, the GO method of Section 2 is used. An incident field of $\hat{\mathbf{e}}_i = \hat{\boldsymbol{\theta}}_f$ polarization produces an aperture reflected field of the following polarization [see (19.9) and (19.27)]:

$$\begin{aligned} \hat{\mathbf{e}}_r^\theta &= 2(\hat{\mathbf{n}} \cdot \hat{\boldsymbol{\theta}}_f) \hat{\mathbf{n}} - \hat{\boldsymbol{\theta}}_f = 2 \sin\left(\frac{\theta_f}{2}\right) \hat{\mathbf{n}} - \hat{\boldsymbol{\theta}}_f = 2 \sin\left(\frac{\theta_f}{2}\right) \cdot \left(-\hat{\mathbf{r}}_f \cos \frac{\theta_f}{2} + \hat{\boldsymbol{\theta}}_f \sin \frac{\theta_f}{2}\right) - \hat{\boldsymbol{\theta}}_f \\ \Rightarrow \hat{\mathbf{e}}_r^\theta &= -\hat{\mathbf{r}}_f \left(2 \sin \frac{\theta_f}{2} \cdot \cos \frac{\theta_f}{2}\right) - \hat{\boldsymbol{\theta}}_f \left(1 - 2 \sin^2 \frac{\theta_f}{2}\right) = -\hat{\mathbf{r}}_f \sin \theta_f - \hat{\boldsymbol{\theta}}_f \cos \theta_f. \end{aligned} \quad (19.35)$$

Similarly, an incident field of $\hat{\mathbf{e}}_i = \hat{\boldsymbol{\phi}}_f$ polarization produces an aperture reflected field of the following polarization:

$$\hat{\mathbf{e}}_r^\phi = -\hat{\boldsymbol{\phi}}_f. \quad (19.36)$$

Transforming (19.35) and (19.36) to rectangular (x and y) coordinates at the aperture plane gives:

$$\begin{aligned} \hat{\mathbf{e}}_r^\theta &= -\hat{\mathbf{x}} \cos \varphi_f - \hat{\mathbf{y}} \sin \varphi_f, \\ \hat{\mathbf{e}}_r^\phi &= +\hat{\mathbf{x}} \sin \varphi_f - \hat{\mathbf{y}} \cos \varphi_f. \end{aligned} \quad (19.37)$$

Superimposing the contributions of the $\hat{\boldsymbol{\theta}}_f$ and $\hat{\boldsymbol{\phi}}_f$ components of the field in (19.32) to the aperture field x and y components produces

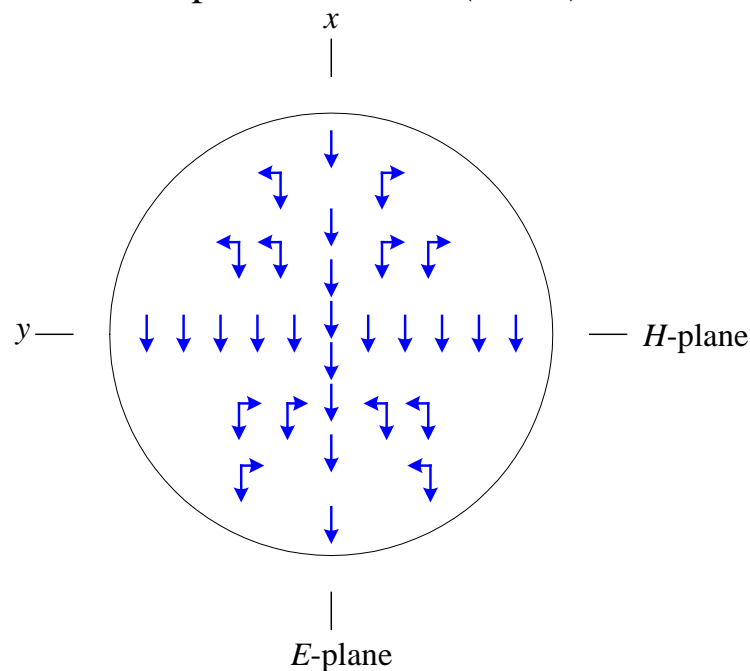
$$\mathbf{E}_a(\theta_f, \varphi_f) = E_m \frac{e^{-j\beta 2F}}{r_f} \times \left\{ -\hat{\mathbf{x}} \left[C_E(\theta_f) \cos^2 \varphi_f + C_H(\theta_f) \sin^2 \varphi_f \right] - \hat{\mathbf{y}} \left[C_E(\theta_f) - C_H(\theta_f) \right] \sin \varphi_f \cdot \cos \varphi_f \right\}. \quad (19.38)$$

In (19.38), the magnitude and phase of the vector are expressed as in (19.22). Note that a y -component appears in the aperture field, despite the fact that the feed generates only E_x field. This is called **cross-polarization**. If the feed has rotationally symmetric pattern, i.e. $C_E(\theta_f) = C_H(\theta_f)$, there is no cross-polarization. From equation (19.38), it is also obvious that cross-polarization is zero at $\varphi_f = 0^\circ$ (E -plane) and at $\varphi_f = 90^\circ$ (H -plane). Cross-polarization is maximum at $\varphi_f = 45^\circ, 135^\circ$. Cross-polarization in the aperture means cross-polarization of the far field, too. Cross-polarization is usually unwanted because it leads to polarization losses depending on the transmitting and receiving antennas.

It is instructive to examine (19.38) for a specific simple example: reflector antenna fed by a very short x -polarized electric dipole. Its principal-plane patterns are $C_E(\theta_f) = \cos \theta_f$ and $C_H(\theta_f) = 1$. Therefore, it generates the following aperture field:

$$\mathbf{E}_a = E_m \frac{e^{-j\beta 2F}}{r_f} \left[-\hat{\mathbf{x}}(\cos \theta_f \cos^2 \varphi_f + \sin^2 \varphi_f) - \hat{\mathbf{y}}(\cos \theta_f - 1) \sin \varphi_f \cos \varphi_f \right]. \quad (19.39)$$

An approximate plot of the aperture field of (19.39) is shown below.



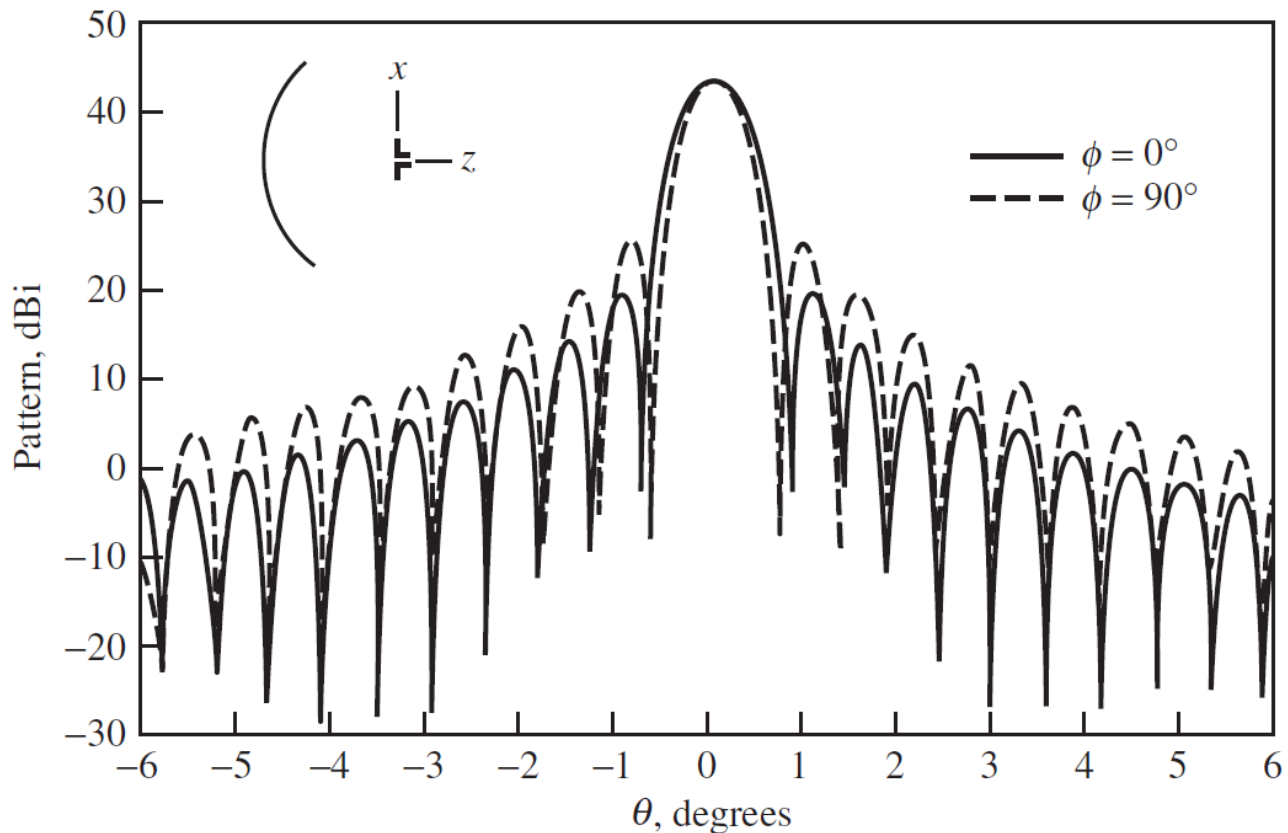
We also note that cross-polarization decreases as the ratio F / D increases. This follows from (19.4), which gives the largest feed angle $(\theta_f)_{\max} = \theta_0$. As F / D increases, θ_0 decreases, which makes the cross-polarization term in (19.39) smaller. Unfortunately, large F / D ratios are not very practical.

Finally, we add that a similar analysis for a y -polarized small dipole feed leads to an expression for the aperture field similar to the one in (19.39) but with a polarization vector

$$\hat{\mathbf{e}}_a = \frac{\hat{\mathbf{x}} \sin \varphi_f \cos \varphi_f (1 - \cos \theta_f) - \hat{\mathbf{y}} (\cos \theta_f \sin^2 \varphi_f + \cos^2 \varphi_f)}{\sqrt{1 - \sin^2 \theta_f \sin^2 \varphi_f}}. \quad (19.40)$$

An example is presented in W.L. Stutzman, G. Thiele, *Antenna Theory and Design*, of an axisymmetric parabolic reflector with diameter $D = 100\lambda$ and $F / D = 0.5$, fed by a half-wavelength dipole located at the focus.

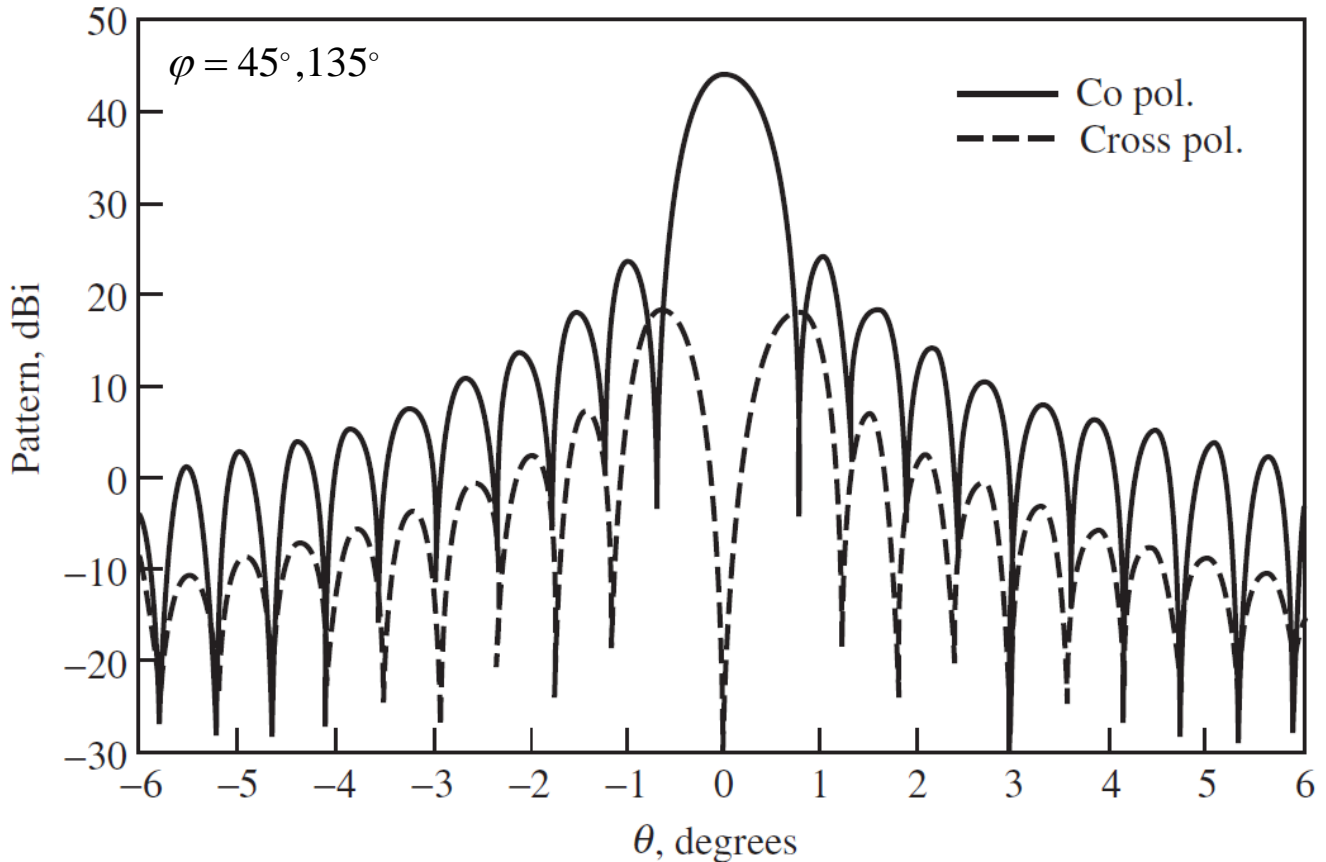
CO-POLARIZATION



(a) Principal plane patterns.

[Stutzman&Thiele]

CROSS-POLARIZATION



[Stutzman&Thiele]

The results above are obtained using commercial software (GRASP) using PO methods (surface current integration).

Cross-polarization of reflectors is measured as the ratio of the peak cross-polarization far-field component to the peak co-polarization far field. For example, the above graph shows a cross-polarization level of $XPOL = -26.3$ dB.

6. Offset parabolic reflectors

One disadvantage of the focus-fed reflector antennas is that part of the aperture is blocked by the feed. To avoid this, offset-feed reflectors are developed, where the feed antenna is away from the reflector's aperture. The reflectors are made as *a portion of* the so-called *parent reflector* surface. The price to pay is the increase of $XPOL$. That is why such reflectors are usually fed with primary feeds of rotationally symmetrical patterns, i.e. $C_E \approx C_H$, which effectively eliminates cross-polarization.

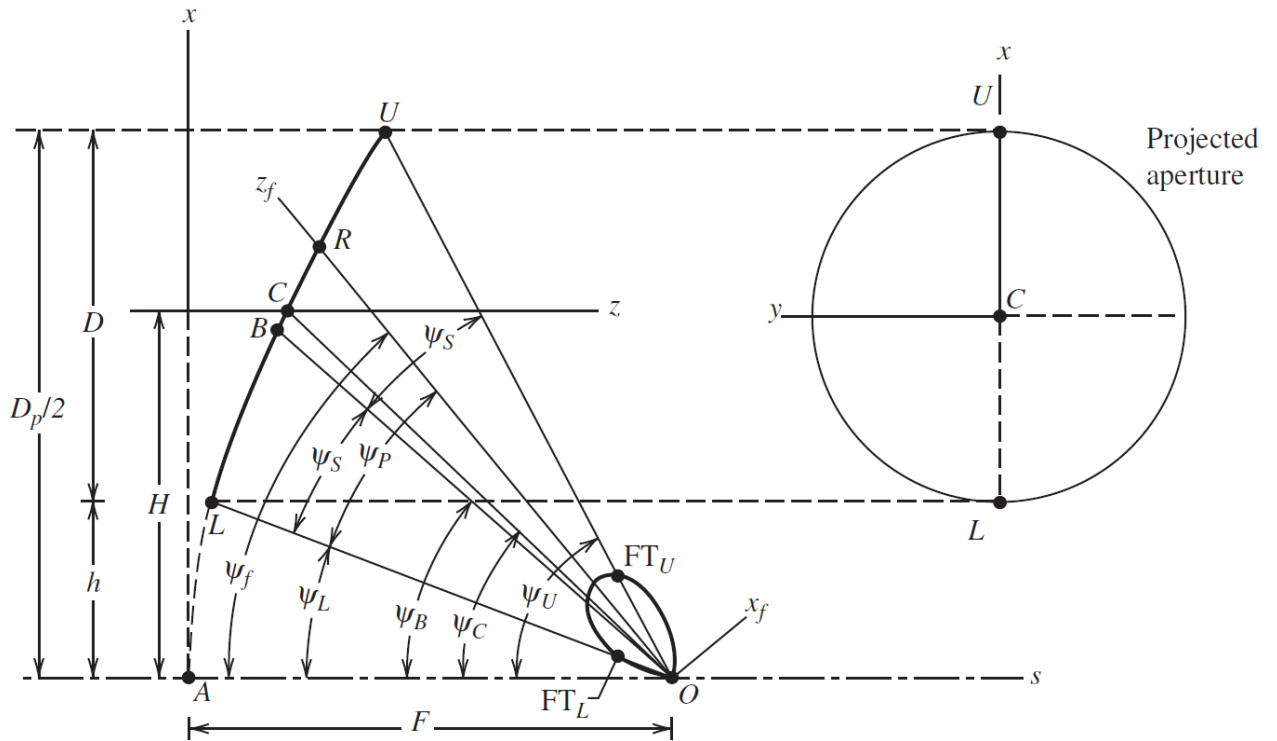
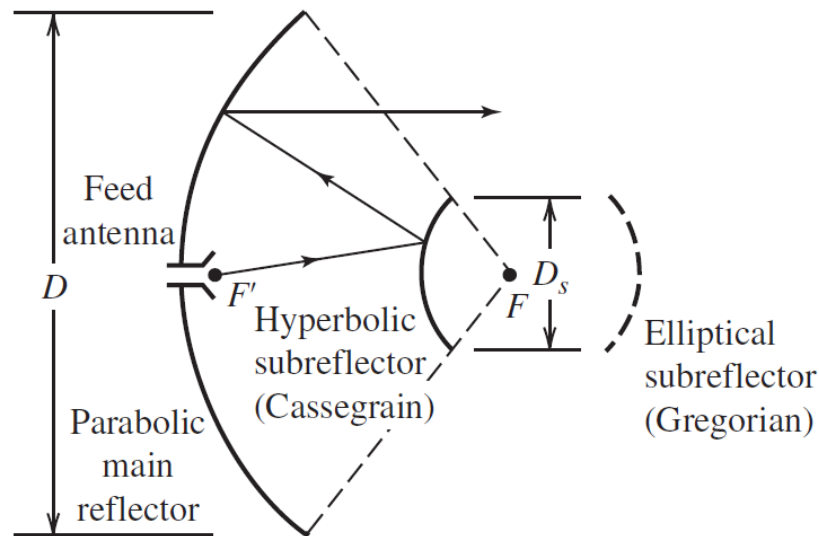


Figure 9-31 Geometry of the offset parabolic reflector of diameter D and focal length F . The axis of symmetry s bisects the parent parabolic curve of diameter D_p . Note that the axisymmetric case occurs when $H = 0$.

[Stutzman&Thiele]

The analysis techniques given in the previous sections are general and can be applied to these reflectors, too. Generally, the PO method (surface currents integration) is believed to yield better accuracy. Both, the PO and the GO methods, are accurate only at the main beam and the first couple of side-lobes.

Offset reflectors are popular for antenna systems producing *contoured beams*. A contoured beam is a beam, the cross-section (or footprint) of which has a shape that conforms to a desired Earth region such as a country or a continent. To obtain such beams, multiple primary feeds (usually horns) are needed to illuminate the reflector at different angles. Such multiple-antenna feeds may constitute a significant obstacle at the antenna aperture and offset reflectors are indeed necessary.



[Stutzman&Thiele]

7. Dual-reflector antennas

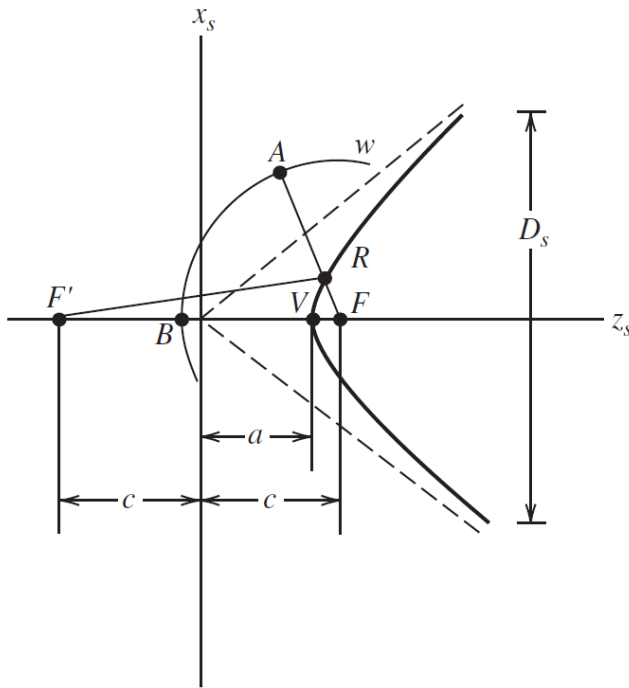
The dual-reflector antenna consists of two reflectors and a feed antenna. The feed is conveniently located at the apex of the main reflector. This makes the system mechanically robust, the transmission lines are shorter and easier to construct (especially in the case of waveguides). The virtual focal point F is the point from which the rays transmitted toward the reflector appear to emanate after reflection from the subreflector.

The most popular dual reflector is the axisymmetric *Cassegrain* antenna. The main reflector is parabolic and the *subreflector is hyperbolic* (convex).

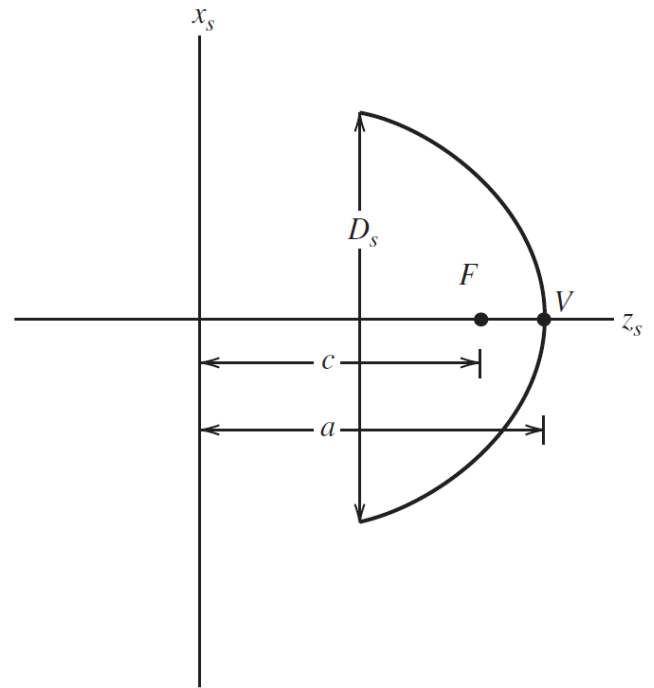
A second form of the dual reflector is the *Gregorian* reflector. It has a concave *elliptic subreflector*. The Gregorian subreflector is more distant from the main reflector and, thus, it requires more support.

Dual-reflector antennas for Earth terminals have another important advantage beside the location of the main feed. They have almost no spillover toward the noisy ground, as do the single-feed reflector antennas. Their spillover (if any) is directed toward the much less noisy sky region. Both, the Cassegrain and the Gregorian reflector systems have their origins in optical telescopes and are named after their inventors.

The subreflectors are rotationally symmetric surfaces obtained from the curves shown below (a hyperbola and an ellipse).



(a) Hyperbolic subreflector.



(b) Elliptical subreflector.

[Stutzman&Thiele]

The subreflector is defined by its diameter D_s and its eccentricity e . The shape (or curvature) is controlled by the eccentricity:

$$e = \frac{c}{a} \begin{cases} > 1, & \text{hyperbola} \\ < 1, & \text{ellipse} \end{cases} \quad (19.41)$$

Special cases are

- $e = \infty$, straight line (plane)
- $e = 0$, circle (sphere)
- $e = 1$, parabola

Both, the ellipse and the hyperbola, are described by the equation

$$\frac{z_s^2}{a^2} - \frac{x_s^2}{c^2 - a^2} = 1. \quad (19.42)$$

The function of a hyperbolic subreflector is to convert the incoming wave from a feed antenna located at the focal point F' to a spherical wave front w that appears to originate from the virtual focal point F . This means that the optical path from F' to w must be constant with respect to the angle of incidence:

$$\overline{F'R} + \overline{RA} = \overline{F'V} + \overline{VB} = \underbrace{c + a}_{\overline{F'V}} + \overline{VB}. \quad (19.43)$$

Since

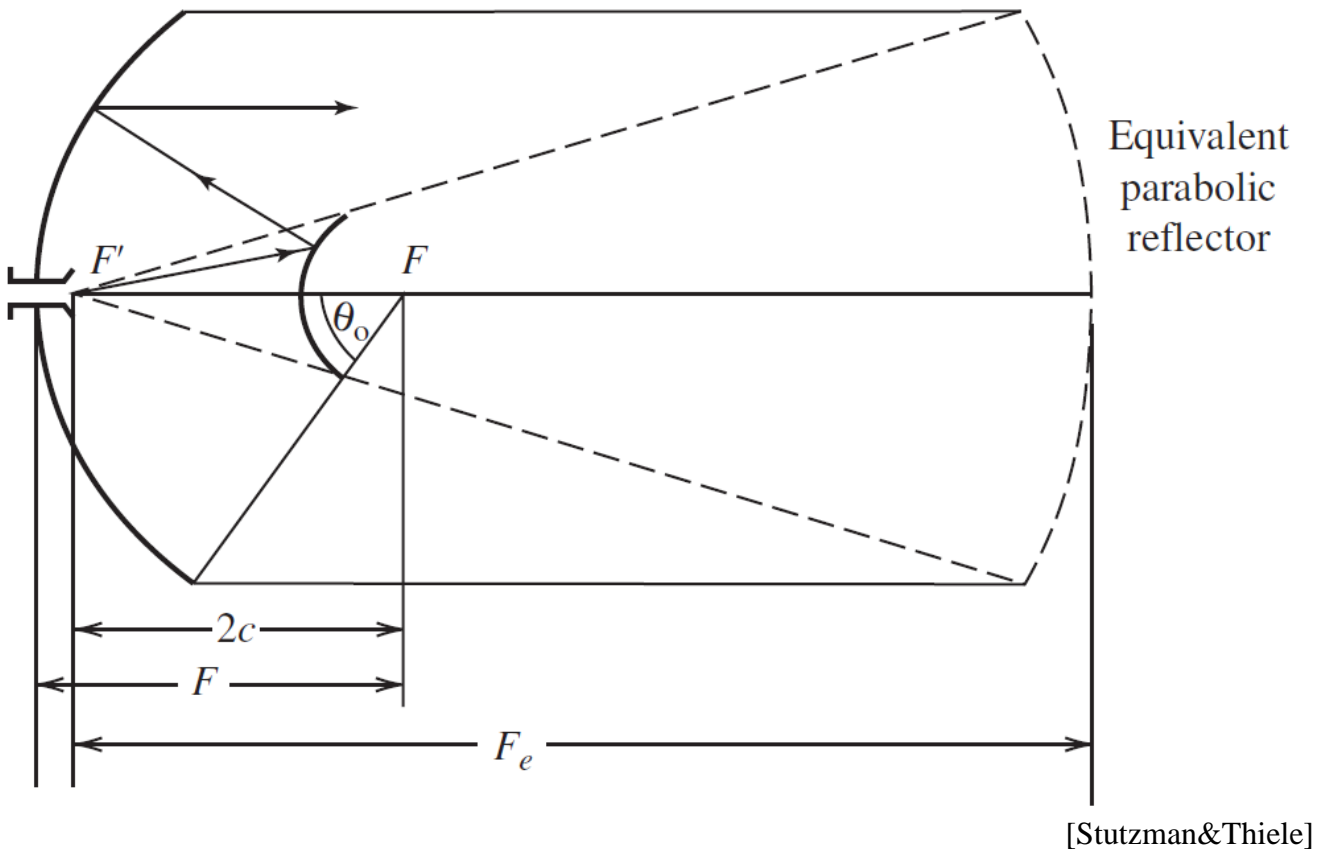
$$\overline{RA} = \overline{FA} - \overline{FR} = \overline{FB} - \overline{FR}, \quad (19.44)$$

($\overline{FA} = \overline{FB}$ because the reflected wave must be spherical)

$$\Rightarrow \overline{F'R} - \overline{FR} = c + a - (\overline{FB} - \overline{VB}) = c + a - (c - a) = 2a. \quad (19.45)$$

Note: Another definition of a hyperbola is: a hyperbola is the locus of a point that moves so that the difference of the distances from its two focal points, $\overline{F'R} - \overline{FR}$, is equal to a constant, $2a$.

The dual axisymmetric Cassegrain reflector can be modeled as a single equivalent parabolic reflector as shown below.



The equivalent parabola has the same diameter, $D_e = D$, but its focal length is longer than that of the main reflector:

$$F_e = \left(\frac{e+1}{e-1} \right) \cdot F = M \cdot F. \quad (19.46)$$

Here, $M = (e + 1) / (e - 1)$ is called *magnification*.

The increased equivalent focal length has several advantages:

- less cross-polarization;
- less spherical-spread loss at the reflector's rim, and therefore, improved aperture efficiency.

The synthesis of dual-reflector systems is an advanced topic. Many factors are taken into account when *shaped* reflectors are designed for improved aperture efficiency. These are: minimized spillover, less phase error, improved amplitude distribution in the reflector's aperture.

8. Gain of reflector antennas

The maximum achievable gain for an aperture antenna is

$$G_{\max} = D_u = \frac{4\pi}{\lambda^2} A_p. \quad (19.47)$$

This gain is possible only if the following is true: uniform amplitude and phase distribution, no spillover, no ohmic losses. In practice, these conditions are not achievable, and the effective antenna aperture is less than its physical aperture:

$$G = \varepsilon_{ap} D_u = \frac{4\pi}{\lambda^2} \varepsilon_{ap} A_p, \quad (19.48)$$

where $\varepsilon_{ap} \leq 1$ is the aperture efficiency. The aperture efficiency is expressed as a product of sub-efficiencies:

$$\varepsilon_{ap} = e_r \varepsilon_t \varepsilon_s \varepsilon_a, \quad (19.49)$$

where:

- e_r is the radiation efficiency (loss),
- ε_t is the aperture taper efficiency,
- ε_s is the spillover efficiency, and
- ε_a is the achievement efficiency.

The taper efficiency can be found using the directivity expression for aperture antennas (see Lecture 17, Section 5):

$$D_0 = \frac{4\pi}{\lambda^2} \frac{\left| \iint_{S_A} \mathbf{E}_a ds' \right|^2}{\iint_{S_A} |\mathbf{E}_a|^2 ds'}. \quad (19.50)$$

$$\Rightarrow A_{eff} = \frac{\left| \iint_{S_A} \mathbf{E}_a ds' \right|^2}{\iint_{S_A} |\mathbf{E}_a|^2 ds'}. \quad (19.51)$$

$$\Rightarrow \varepsilon_t = \frac{A_{eff}}{A_p} = \frac{1}{A_p} \frac{\left| \iint_{S_A} \mathbf{E}_a ds' \right|^2}{\iint_{S_A} |\mathbf{E}_a|^2 ds'}. \quad (19.52)$$

Expression (19.52) can be written directly in terms of the known feed antenna pattern. If the aperture is circular, then

$$\varepsilon_t = \frac{1}{\pi a^2} \frac{\left| \int_0^{2\pi} \int_0^a \mathbf{E}_a(\rho', \varphi') \rho' d\rho' d\varphi' \right|^2}{\int_0^{2\pi} \int_0^a |\mathbf{E}_a(\rho', \varphi')|^2 \rho' d\rho' d\varphi'}. \quad (19.53)$$

Substituting $\rho' = r_f \sin \theta_f = 2F \tan(\theta_f / 2)$ and $d\rho' / d\theta_f = r_f$ in (19.53) yields

$$\varepsilon_t = \frac{4F^2}{\pi a^2} \frac{\left| \int_0^{2\pi} \int_0^{\theta_o} \mathbf{F}_f(\theta_f, \varphi') \tan\left(\frac{\theta_f}{2}\right) d\theta_f d\varphi' \right|^2}{\int_0^{2\pi} \int_0^{\theta_o} |\mathbf{F}_f(\theta_f, \varphi')|^2 \sin \theta_f d\theta_f d\varphi'}. \quad (19.54)$$

All that is needed to calculate the taper efficiency is the feed pattern $\mathbf{F}_f(\theta_f, \varphi')$.

If the feed pattern extends beyond the reflector's rim, certain amount of power is not redirected by the reflector, i.e., it is lost. This power-loss is referred to as *spillover*. The spillover efficiency measures that portion of the feed pattern, which is intercepted by the reflector relative to the total feed power:

$$\varepsilon_s = \frac{\int_0^{2\pi} \int_0^{\theta_0} |\mathbf{F}_f(\theta_f, \varphi')|^2 \sin \theta_f d\theta_f d\varphi'}{\int_0^{2\pi} \int_0^{\pi} |\mathbf{F}_f(\theta_f, \varphi')|^2 \sin \theta_f d\theta_f d\varphi'}. \quad (19.55)$$

The reflector design problem includes a trade-off between aperture taper and spillover when the feed antenna is chosen. Taper and spillover efficiencies are combined to form the so-called *illumination efficiency* $\varepsilon_i = \varepsilon_t \varepsilon_s$. Multiplying (19.54) and (19.55), and using $a = 2F \tan(\theta_0 / 2)$ yields

$$\varepsilon_i = \frac{D_f}{4\pi^2} \cot^2 \frac{\theta_0}{2} \left| \int_0^{2\pi} \int_0^{\theta_0} \mathbf{F}_f(\theta_f, \varphi') \tan \frac{\theta_f}{2} d\theta_f d\varphi' \right|^2. \quad (19.56)$$

Here,

$$D_f = \frac{4\pi}{\int_0^{2\pi} \int_0^{\pi} |\mathbf{F}_f(\theta_f, \varphi')|^2 \sin \theta_f d\theta_f d\varphi'}, \quad (19.57)$$

is the directivity of the feed antenna. An ideal feed antenna pattern would compensate for the spherical spreading loss by increasing the field strength as θ_f increases, and then would abruptly fall to zero in the direction of the reflector's rim in order to avoid spillover:

$$F_f(\theta_f, \varphi') = \begin{cases} \frac{\cos^2(\theta_0 / 2)}{\cos^2(\theta_f / 2)}, & \theta_f \leq \theta_0 \\ 0, & \theta_f > \theta_0 \end{cases} \quad (19.58)$$

This ideal feed is not realizable. For practical purposes, (19.56) has to be optimized with respect to the edge-illumination level. The function specified by (19.56) is well-behaved with a single maximum with respect to the edge-illumination.

The achievement efficiency ε_a is an integral factor including losses due to: random surface error, cross-polarization loss, aperture blockage, reflector phase error (profile accuracy), feed phase error.

A well-designed and well-made aperture antenna should have an overall

aperture efficiency of $\varepsilon_{ap} \approx 0.65$ or more, where “more” is less likely.

The gain of a reflector antenna also depends on **phase errors**, which theoretically should not exist but are often present in practice. Any departure of the phase over the virtual aperture from the uniform distribution leads to a significant decrease of the directivity. For paraboloidal antennas, phase errors result from:

- displacement of the feed phase centre from the focal point;
- deviation of the reflector surface from the paraboloidal shape, including surface roughness and other random deviations;
- feed wave fronts are not exactly spherical.

Simple expression has been derived¹ to predict with reasonable accuracy the loss in directivity for rectangular and circular apertures when the peak value of the aperture phase deviations is known. Assuming that the maximum radiation is along the reflector’s axis, and assuming a **maximum aperture phase deviation** m , the ratio of the directivity without phase errors D_0 and the directivity with phase errors D is given by

$$\frac{D}{D_0} \approx \left(1 - \frac{m^2}{2}\right)^2. \quad (19.59)$$

The maximum phase deviation m is defined as

$$|\Delta\phi| = |\phi - \bar{\phi}| \leq m, \quad (19.60)$$

where ϕ is the aperture’s phase function, and $\bar{\phi}$ is its average value. The aperture phase deviation should be kept below $\pi/8$ if the gain is not to be affected much. Roughly, this translates into surface profile deviation from the ideal shape (e.g. paraboloid) of no more than $\lambda/16$.

¹ D.K. Cheng, “Effects of arbitrary phase errors on the gain and beamwidth characteristics of radiation pattern,” *IRE Trans. AP*, vol. AP-3, No. 3, pp. 145-147, July 1955.